C12ORF57: a novel principal regulator of synaptic AMPA currents and excitatory neuronal homeostasis

Ruiji Jiang[1**], Malek Chouchane[1], Ching Moey[2], Jens Bunt[2], Jiang Li[1], Fowzan Alkuraya[4], Eman Alobeid[5], Linda Richards[2,5,] Erik Ullian[6], Elliott Sherr[1]**

1. University of California San Francisco Department of Neurology, San Francisco, CA United States
2. The University of Queensland, Queensland Brain Institute, Brisbane, Australia
3. King Faisal Specialist Hospital and Research Center, Department of Genetics, Riyadh, Saudi Arabia
4. Department of Genetics, King Faisal Specialist Hospital and Research Center, Riyadh, Saudi Arabia
5. Washington University in Saint Louis, Department of Neuroscience, St Louis, MO United States
6. University of California San Francisco, Department of Ophthalmology, San Francisco, CA, United States

.

Abstract

Biallelic recurrent loss of function mutations in *C12ORF57*, a novel open reading frame, underlie Temtamy syndrome (TS)—a neurodevelopmental disorder characterized by dysgenesis of the corpus callosum, epilepsy, and severe intellectual disability. To study the heretofore unknown function of this gene, we used a knockout (KO) mouse model of its murine ortholog, *Grcc10*. *Grcc10* KO mice exhibit the characteristic phenotypic features seen in human TS patients,

including increased epileptiform activity. Consistent with this propensity for seizures, hippocampal neurons in these mice show significantly increased AMPA receptor expression levels and higher amplitude of miniature excitatory postsynaptic currents (mEPSCs). We also find that GRCC10/C12ORF57 modulates the activity of calcium/calmodulin dependent kinase 4 (CAMK4) and regulates the expression of CREB and ARC, which are involved in synaptic scaling of AMPA receptors. Through multiple lines of inquiry, we establish that C12ORF57/GRCC10 plays a central modulatory role in synaptic homeostasis and uncover a novel mechanism for neuronal excitatory tuning.

Keywords: Temtamy syndrome, C12ORF57, epilepsy, ASD, CAMK4, CREB, ARC, neuronal homeostasis, AMPA receptors

Introduction

C12ORF57 is a three exon gene encoding a highly conserved 126 amino acid, 13 kD protein that is abundantly expressed in human fetal and postnatal brain (1,2). Recent linkage and sequencing analyses have identified a recurrent autosomal recessive mutation in the start codon (c.1A>G, p.1M>V) of *C12ORF57* as the cause of Temtamy syndrome (TS), an autism and intellectual disability (ID) disorder characterized by ocular coloboma, dysgenesis of the corpus callosum and medically intractable seizures (1–5). This syndrome was initially reported in Middle Eastern populations but subsequently also noted in other countries (3,6–8). The above mentioned mutation is observed throughout the Middle East and is the single most common cause of recessive ID and developmental delay in Saudi Arabia, accounting for greater than 1% of intellectual disability with genetic cause in these cohorts (2,3). Despite the widespread nature of this mutation among affected populations and evolutionary conservation suggesting an important biological function, currently

45 there is little known about its role in normal neuronal development and homeostasis. This is
46 because C12ORF57 lacks homology to any known vertebrate protein, making it difficult to predict
47 its function (**Supplemental Figure 1**) (2). To discover the function of this novel gene, we
48 generated and analyzed the consequences of homozygous knockout model of its murine ortholog,
49 *Grcc10,* with which it shares 99.2% amino acid identity (**Supplemental Figure 1**).

50 We show that *Grcc10* knockout (KO) mice recapitulate many of the phenotypes found in human
51 TS patients, notably epilepsy and corpus callosum anomalies, making it a useful model in which
52 to study the function of this gene. Using biochemical (including yeast-2-hybrid interactions) and
53 electrophysiological assays, we examine the potential mechanisms by which C12ORF57/GRCC10
54 regulates synaptic excitability. We analyze its interaction with the neuronal homeostasis protein,
55 calcium calmodulin dependent kinase IV (CAMK4), as well as its regulation of CREB, Fos, and
56 ARC, which are implicated in the synaptic scaling of AMPA receptors (9). Taken together, our
57 data show for the first time, that C12ORF57 is a central regulator of synaptic homeostasis, and
58 also reveal a novel mechanism of neuronal excitatory tuning.

59 **Results**

60 **Grcc10 loss of function in mice recapitulates Temtamy syndrome phenotypes**

61 When examined by RT-PCR, the *C12ORF57* transcript was not detected in primary fibroblasts
62 from patients homozygous for the most common c.1 A>G variant , suggesting that their phenotype
63 was consistent with a complete loss of function (LoF) (**Figure 1a**) (2,3). To model this
64 homozygous inactivation of *C12ORF57* in human disease, we generated a transgenic mouse line
65 (*Grcc10<tm1.1(KOMP)Vlcg>*) carrying a beta galactosidase-containing cassette that
66 constitutively disrupts the *Grcc10* gene (*Grcc10* KO). *Grcc10* +/+ (WT), +/- (Het) and -/- (KO)

littermates were born with the expected 1:2:1 Mendelian ratios from heterozygote pairs (X=.014, dF=2, p=.99, Chi-Square, n=154) **(Figure 1b**). *Grcc10 -/-* pups had high postweaning mortality compared to WT and Het littermates as early as postnatal day 3 (P3) (X=.014, df=2, p=.00013, Chi-Square, n=91), with the majority of animals dying before P2 (**Figure 1b**). *Grcc10* KO mice that survived until weaning age showed significantly diminished physical growth compared to their WT and Het littermates (11.71±0.11g vs. 4.15±0.99g, respectively, p<.00001 t=33.07, df=8.18, N=5, Welch's T-Test), suggesting that *Grcc10* is also crucial for health and survival (**Figure 1c**).

Since our previous work associating *C12ORF57* with ID, ASD, and epilepsy, and its high expression in human fetal brain tissue strongly suggests a crucial role in normal brain development, we first investigated *Grcc10* expression in early mouse brain development using *in situ* hybridization on late embryonic days (E)15 and 18 (E15, E18) and P0 and P10 .(1,3) We observed that *Grcc10* is broadly expressed in many brain regions at all ages examined. At E15, it is specifically localized to the cortical plate, glial wedge, and the dorsal ventricular zone. At E18, we observed higher expression in the cortex, hippocampus, and thalamus that was maintained until P10 (**Figure 1d**). Interrogation of Allen Brain Atlas cell and region-specific RNA-seq also shows global expression across multiple brain areas and neuronal cell types (**Supplemental Figure 2**). The widespread expression of *Grcc10* in the developing cortex suggests that *Grcc10* may play an early and central role in cortical development. In addition, since previous studies showed that disrupted cortical lamination is linked to ASD, ID and epilepsy (REF), we examined whether this was the case in *Grcc10* KO mice by performing immunohistochemistry on P0 murine cortical slices using previously validated upper- and lower-layer markers *Satb2* and *Ctip2* respectively(10,11). We observed no difference in the number of Satb2 WT (1403.00±89.09

90 cells/HPF) versus KO (1498.20±40.14, p=.36, t=.95, df=10, Welch's tailed T-test) or Ctip2
91 neurons in WT (610.43±31.00) versus KO (633.17±41.03, p=0.76, t=0.32, df=11, Welch's T-test)
92 or the pattern of lamination of WT and *Grcc10* KO cortices, suggesting that *Grcc10* loss of
93 function does not impair gross cortical architecture or layering (**Supplemental Figure 3**).

94 Our *Grcc10* -/- mice share a shortened corpus callosum structure similar to what is found in
95 patients with Temtamy syndrome. In P0 KO mice, corpus callosum length was shorter
96 (792.81±39.15 µm, p=.017, F=6.41, df=2. N=6, ANOVA) when compared to their WT
97 (984.53±12.23µm, p=.023, df=9, Tukey post-hoc test), and heterozygous littermates
98 (931.89±47.73µm) thought not statistically significantly so (p=.092, q=3.391, DF=9, Tukey post-
99 hoc test). The corpus callosum cross sectional area in these P0 KO mice was also reduced
100 (154859.22±8441.27µm^2) (p=.0058 ,ANOVA, F=9.65, df=2 N=6) compared to WT
101 (199602.27±8702.73µm^2) (p=.012,q=3.546, df=9, N=3, Tukey post-hoc test) and Het mice
102 (200644.93±6764.12µm^2, p=.010 q=3.628, DF=2, N=3, Tukey post-hoc test). Rostral to caudal
103 cortical length between KO (1625.01±30.49µm) and WT (1706.25 ±56.16 µm,) or Het
104 (1709.39±63.84 µm p=.29, ANOVA, F=1.337, df=2, N=6) was not significantly different (**Figure**
105 **1e**).

106 Patients harboring *C12ORF*57 homozygous or biallelic mutant variants have a high rate of epilepsy
107 that is refractory in many cases (3,4). We have observed *Grcc10* KO mice displaying spontaneous
108 seizure activity (**Supplemental Video 1**), but their early mortality and small size prevented us
109 from conducting EEG monitoring. To assess seizure susceptibility, we tested whether these mice
110 are more susceptible to pharmacologically induced seizures. We performed intra-peritoneal kainic
111 acid injection in P21 *Grcc10* KO, Het and WT mice, and scored their behaviors indicative of

112 seizures based on the Racine scale of 1-5 (**Figure 1f**) (12–15). We observed that all animals
113 presented with seizures following kainic acid, but not carrier injections. *Grcc10* KO mice reached
114 clinically severe stages (=>5) significantly faster (9.44±1.33 min,p<.0001, 2-way ANVOA
115 F=46.34, F=764.66 N=4) than *Grcc10* WT (36.33±2.84 min, p<.0001, N=6, Tukey post-hoc test)
116 or Het littermates (20.74±1.82 min, N=5 p<.0001, Tukey post-hoc test) (**Figure 1g**). These data
117 suggest that *Grcc10* KO mice have higher underlying susceptibility to induced seizures, analogous
118 to the increased rate of epilepsy seen in human Temtamy syndrome patients.

119 **Grcc10 loss of function causes an increase in AMPA mediated mEPSCs**

120 We next asked what synaptic changes may mediate the severe seizure activity seen in our mouse
121 model. We hypothesized that we would be able to see increased neuronal excitability through
122 AMPA (α-amino-3-hydroxy-5-methyl-4-isoxazolepropionic acid) mediated currents based on
123 substantial evidence from many animal models that shows that these receptors are key mediators
124 of seizure spread and epileptogenesis (16,17). We measured electrophysiological parameters in
125 *Grcc10* KO neurons by first assessing spontaneous AMPA mediated miniature excitatory
126 postsynaptic currents (mEPSC) using whole cell recordings in isolated excitatory hippocampal
127 neurons from E18 *Grcc10* WT, and KO mice on day *in vitro* (DIV) 14-18. We observed that
128 AMPA-mediated mEPSCs recorded from *Grcc10* KO neurons have a significantly higher mean
129 amplitude than mEPSCs recorded from *Grcc10* WT neurons (35.81±0.90 pA vs .15.49±0.29 pA,
130 respectively, p<.0001, F=367, df=2, N=5 neurons per genotype, ANOVA with Tukey post-hoc
131 test) (**Figure 2a-c**). These data support the hypothesis that *Grcc10* loss of function causes an
132 increase in AMPA-mediated mEPSC amplitudes. In contrast, NMDA amplitude and frequency
133 were not significantly different between WT and KO neurons (13.84±3.93 pA vs. 12.92±2.92 pA,

134 p=0.20, t=1.27, df=301.4, N=5, Welch's T-test) (**Figure 2d**). GABA current amplitude was also
135 not significantly different between WT and KO neurons (13.78±3.32pA vs. 15.56±8.37 pA,
136 (p=.16, t=1.41, df=137, N=5 Welch's T-test) (**Figure 2e**). To confirm that the loss of
137 C12ORF57/GRCC10 was a necessary and sufficient cause of the increase in AMPA mEPSC
138 activity in these cultured neurons, we sought to rescue the *Grcc10* KO neurons using lentiviral
139 vector containing *C12ORF57-P2A-GFP* construct under *Syn2* translational control with a *GFP*
140 only lentivirus serving as a control (**Supplemental Figure 4**). We transfected E18 *Grcc10* KO
141 neurons on DIV 7 with both the construct and a *GFP* only vector and compared their
142 electrophysiology profiles on DIV14-18 with WT lentiviral infected *GFP* controls. *Grcc10* KO
143 neurons transfected with *C12ORF57* had decreased mEPSC amplitude compared to *GFP*-
144 transfected KO neurons (18.27±0.47 pA vs. 38.93±0.56 pA, respectively, p<.0001) and had no
145 statistically significant differences in mEPSC amplitude compared to *GFP* transfected WT neurons
146 (15.50±0.32 pA ; p=.57, t=0.17, df=137.2 ANOVA, N=4) (**Figure 2f**). Frequency of AMPA
147 mEPSC also decreased in *C12ORF57*-transfected compared to *GFP*-transfected KO neurons
148 (5.46± 0.61 events/sec vs. 22.46 ±0.47 events/sec, respectively, p<.0001, ANOVA with Tukey
149 post-hoc test, F=85.3, df=2, N=5). *C12ORF57*-transfection rescued the phenotype in KO neurons
150 (19.06±0.81 events/sec, P<.0001, ANOVA Tukey post-hoc test, N=5), which were now
151 comparable to WT neurons (5.21±1.31 events/sec p>.999, ANOVA with Tukey post-hoc, df=2,
152 N=5) (**Figure 2g**). These data suggest that C12ORF57 specifically modulates post-synaptic
153 AMPA current and is sufficient to rescue the excessively increased excitability phenotype seen in
154 *Grcc10* KO neurons and is necessary for normal neuronal electrophysiology.

155 **Loss of *Grcc10/C12ORF57* leads to an increase in surface AMPA receptor localization and**
156 **impairs excitatory homeostatic synaptic down-scaling after blocking GABA receptors.**

157 Given our findings of increased AMPA current in *Grcc10-/-* neurons we hypothesized that loss of
158 *Grcc10/C12ORF57* would result in increased GluA2 surface expression. AMPA receptors are
159 post-synaptic heterotetrameric assemblies of two homologous subunits (GluA1-4), with
160 compositions containing two GluA2 subunits being the most predominant in hippocampal
161 pyramidal neurons and mediating the majority of fast excitatory synaptic transmission in the brain.
162 We stained for membrane bound GluA2 subunits on isolated DIV 17 *Grcc10* WT an KO)
163 pyramidal hippocampal neurons and quantified the fluorescence intensity of GluA2 positive
164 puncta per 50 µm of neuronal processes. We observed an increase in the number of GluA2 puncta
165 (83.72±23.10%,(p=.0024, t=3.62, df=15.32, N=10 per genotype Welch's T-test) and an increase
166 in puncta intensity (102.43±28.66%, p=.0008, t=3.572 df=51.84, N=19 WT, N=35 KO, Welch's
167 T-Test) in *Grcc10* KO neurons compared to WT neurons (**Figure 3a**).

168 We also sought to determine if *Grcc10* KO neurons would be less able to downregulate AMPA
169 current in response to increased excitation, which would be predicted with decreased CAMK4
170 activity in the KO mice. To do this, we measured surface AMPA receptor expression after inducing
171 a chronic increase in postsynaptic activity by treating neurons with bicuculline (a GABA receptor
172 antagonist) for 48 hours and then measuring GluA2 surface expression (19). We observed that, as
173 expected, bicuculline treatment caused a significant decrease in surface GluA2 expression in WT
174 neurons (-907.00±293.20 puncta/HPF, p=.0041, t=3.09, df=32, untreated N=19, treated N=15
175 ,Welch's T-test). In contrast, bicuculline treatment had no significant effect on GluA2 in *Grcc10*
176 KO neurons (-255.0±616.9 puncta/HPF, p=.68, T=.41, df=53, N=19 untreated, N=15 bicuculline
177 treated, Welch's T-Test) (**Figure 3b**). We also observed an increase in dendritic spine density in
178 *in situ Grcc10* KO cortical neurons (1.26+/-0.53 spines/µm) compared to WT cortical neurons
179 0.91+/-0.22 spines/µm, p=.0023, t=3.185, df=57, N=33, Welch's T-Test) (Figure 3C), though

180 spine width was not statistically different between the two neuron types (33.53+/-18.57 vs 34.53+/-
181 19.75, p=.83, t=.198, df=57, N=33, Welch's T-test). These findings suggest that GRCC10 loss of
182 function increases dendritic spine density and GluA2 surface expression and impairs homeostatic
183 synaptic down-scaling of GluA2 and results in higher levels of AMPA expression at synapses both
184 at baseline and under conditions of acute increases in neuronal activity. This data further supports
185 our observation of increased AMPA current in *Grcc10-/-* mouse neurons described in the previous
186 section.

187 **C12ORF57/Grcc10 loss of function causes a decrease in the expression of pCREB, cFOS and**
188 **ARC**

189 Because the loss of C12ORF57 disrupts synaptic AMPA downscaling and current, we sought to
190 determine if there were changes to the negative regulation of AMPA synapses involving CREB
191 and ARC signaling. This is because phosphorylated CREB (p-CREB) regulation of the immediate
192 early gene, *Arc*, is implicated in the synaptic downscaling of AMPA receptors and the regulation
193 of surface GluA2 expression in response to neuronal excitation (9,20–28). To investigate if this
194 pathway is altered in our KO mice, we stained primary hippocampal *Grcc10* WT and KO neurons
195 isolated at E18 at 20 days *in vitro* using an antibody that binds specifically to the Ser133 p-CREB
196 and ARC and measured fluorescence intensity. We observed that KO neurons express a
197 significantly lower level of Ser133-pCREB (-29.80±8.55%, (p=.0008, t=3.66, df=38, N=20,
198 Welch's T-Test) and ARC (-65.79±9.18%, p<.0001, t=7.17, df=38 N=24, Welch's T-Test)
199 compared to WT neurons (**Figure 4a-c**). These data were also supported by western blot findings
200 of decreased pCREB in whole brain lysates of KO mice compared to WT (-31.26±12.47%,
201 (p=.024, t=2.5, df=14.72, N=5, Welch's T-Test) and decreased intermediate early genes ARC (-

202 48.03±8.44%, p=.0036, t=5.69, df=4.36, N=5 Welch's T-Test) and cFOS (-49.94%±10.45,
203 =.0043, t=4.78, df-5.288, N=5, Welch's T-Test) (**Figure 4d-f**). These results suggest that *Grcc10*
204 loss of function leads to a decrease in CREB phosphorylation and decreased expression of ARC
205 and cFOS.

206 To further study the effect of *C12ORF57*/*Grcc10* loss of function on CRE-dependent
207 transcriptional activation, we performed a dual luciferase assay as described by Bellis et al. (29).
208 We transfected both *C12ORF57* WT and KO HEK293T cells with one construct containing
209 *Renilla* luciferase as a reporter of CRE promoter activity and another one expressing firefly
210 luciferase under a constitutive promoter as a control. We observed that KO cells had a significant
211 decrease in normalized CRE-driven *Renilla* luminescence compared to WT cells (-25.40±3.78%,
212 ANOVA, F=20.74, p<.0001, Tukey post-hoc test, p=.019, N=3 per experimental condition).
213 Moreover, transfection of *C12ORF57*-/- cells with C12ORF57 restored CRE driven luciferase
214 signal to wildtype levels (+27.56±17.10%, p=0.12, Tukey post-hoc test) (**Figure 4g**). These data
215 show that loss of C12ORF57 reduces CRE-dependent transcriptional activation, potentially
216 impacting the negative regulatory elements upstream of AMPA, CREB and ARC.

217 **C12ORF57 enhances CAMK4 activity through interactions with its autoinhibitory domain**

218 The lack of significant homology of GRCC10 to any known protein impaired our ability to predict
219 its cellular mechanisms *a priori*. To bypass this limitation, we analyzed the GRCC10 protein
220 interactome using two independent unbiased Yeast 2-hybrid screens utilizing mouse brain libraries
221 (30). Both unbiased genome-wide screens resulted in a single positive clone that encoded the
222 calcium calmodulin associated kinase IV (CAMK4). We conducted direct co-immunoprecipitation
223 of GRCC10 from whole WT and KO mouse brain lysate and confirmed its interaction with

224 CAMK4 in WT lysate which was abolished in KO lysate (**Figure 5a**). Discovery of C12ORF57's
225 interaction with CAMK4 is particularly informative because CAMK4 is a known upstream
226 regulator of both CREB and ARC and plays a role in synaptic downscaling (9,23,31).

227 Given the close association of C12ORF57/GRCC10 with CAMK4, we next investigated whether
228 it plays a role in modulating CAMK4 activity. In prior studies, phosphorylated CAMK4 has been
229 shown to be largely confined to the nucleus. This localization for CAMK4 was shown to be
230 mediated by phosphorylation at amino acid (AA) Thr200 in humans and via Thr196 in mice
231 (26,27,32,33). We measured the expression of CAMK4 in *Grcc10* WT versus KO brains by
232 western blot and observed that differences between total CAMK4 were not significant between
233 WT and KO brains (-0.74 $\pm$0.73%, p=.34, t=1.01, df=6.97, N=6 Welch's T-Test). However, we
234 did see a shift in CAMK4 distribution within the nucleus of KO brains compared to WT brains
235 with significantly less pCAMK4 (-66.66$\pm$6.83%, p=0.0037, F=18.33, df=3, N=5, ANOVA with
236 Tukey) and total CAMK4 (-48.1$\pm$6.73% , p=0.002 F=14.89, N=5, df=3, ANOVA with Tukey post-
237 hoc test). We saw the opposite shift in cytoplasmic fraction, where KO brains showed an increase
238 in total CAMK4 (+31.6$\pm$20.69%, p=.0035 2-way ANOVA, F=5.50, DF=2, N=6) compared to WT,
239 and a similar, though not statistically significant, decrease in pCAMK4 (+31.87$\pm$19.51, p=.1848,
240 N=6, Tukey post-hoc test) (**Figure 5b-g**). These results suggest that loss of C12ORF57 disrupts
241 the balance of nuclear versus cytoplasmic CAMK4, with increased nuclear phosphorylated
242 CAMK4 in WT brains when compared to KO brains.

243 To further uncover how C12ORF57/GRCC10 interacts with CAMK4 and because we observed
244 changes in CAMK4s phosphorylation and localization with C12ORF57 loss, we investigated the
245 roles of various regulatory domains of CAMK4. We created two modified forms of CAMK4

246 constructs lacking distinct regulatory domains: one which lacks the autoinhibitory domain (AA
247 305-321) (NAI), which binds CAMK4-negative regulatory proteins phosphatase 1 and 2 (PP1 and
248 PP2), and the other lacking the calmodulin binding domain (AA 322-341) (NCB) (**Figure 5h**)(34).
249 We co-transfected these constructs in HEK293T cells with a flag-tagged version of C12ORF57
250 and performed a co-immunoprecipitation assay with CAMK4. We observed that the deletion of
251 the autoinhibitory domain significantly reduced the ability of CAMK4 to bind to C12ORF57-
252 FLAG (-65.76±6.76%, p<.0001, N=8, ANOVA with Tukey post-hoc test) when compared to wild
253 type CAMK4, whereas deletion of the calmodulin binding domain resulted in no significant
254 change in binding (-6.13±6.81%, p=.66, ANOVA with Tukey post-hoc test, N=8) (**Figure 5h-j**).
255 This suggests that the CAMK4 autoinhibitory domain plays a significant role in its interaction with
256 C12ORF57.

257 The association of C12ORF57 with CAMK4's autoinhibitory domain that interacts with protein
258 phosphatases, along with the decrease in pCAMK4 in KO brain nuclei, led us to hypothesize that
259 C12ORF57/GRCC10 could disrupt the activity of phosphatases that modulate CAMK4 activity.
260 To investigate this, we measured *in vitro* CAMK4 kinase activity in the presence or absence of
261 C12ORF57 and/or serine/threonine-protein phosphatase alpha catalytic subunit 1 (PP1CA) using
262 an *in vitro* kinase enzyme system that enables the quantification of ATP consumption by CAMK4
263 via luminescence (31). We found that the addition of PP1CA significantly decreases CAMK4 *in*
264 *vitro* activity by 39.32% (-981.00±75.95 Relative luminesce units, RLU, p=<.0001, ANOVA with
265 Tukey's post-hoc test), which is expected given its negative regulatory activity *in vivo* (**Figure**
266 **5k**). We also found that adding C12ORF57 does not affect CAMK4 kinase activity compared to
267 CAMK4 alone (-66.33±90.83 RLU, p=85, F=448.3, df=6, N=3,p=.95, ANOVA with Tukey's
268 post-hoc test). The presence of both C12ORF57 and PP1CA caused CAMK4 activity to decrease

269 significantly than just PP1CA alone (-681.00±67.39 RLU p>.0001, ANOVA with Tukey's post-
270 hoc test) (**Figure 5k**). This, in conjunction with our previous data, suggests that C12ORF57
271 enhances CAMK4 activity by reducing efficacy of phosphatase inhibition by binding to the
272 autoinhibitory domain of CAMK4 and increasing the relative amount of active phosphorylated
273 CAMK4.

274 *Overexpression of CAMK4* is sufficient to rescue *Grcc10* excitability phenotype.

275 Because we hypothesize that CAMK4 is downstream of C12ORF57/GRCC10, we tested whether
276 overexpression of CAMK4 would be sufficient to rescue the increased AMPA mEPSC phenotype
277 in *Grcc10-/-* neurons. We performed whole cell recordings on isolated excitatory hippocampal
278 neurons from embryonic day 18, *Grcc10* WT, and KO mice on DIV 14-18 that were transfected
279 with a lentivirus carrying a mouse *Camk4-Pp2A-Gfp* fusion under *CMV* promoter control versus
280 an empty vector as a negative control and a *C12ORF57* positive control. *Grcc10* KO neurons
281 transfected with *CAMK4* had AMPA amplitudes statistically significantly lower (p<.0001,
282 F=240.8, dF, 3,N=6, ANOVA) than vector-infected KO neurons (12.54±2.29 pA vs. 46.11± 20.70
283 pA, respectively, p<.0001, Tukey post-hoc test) and equal to WT neurons (12.30±3.52 pA p=.99,
284 N=6, Tukey post-hoc test) and *C12ORF57*-transfected KO neurons (12.55±3.684pA, p=.9987,
285 N=6, Tukey post-hoc test) (**Figure 5l**). These data suggest that CAMK4 is indeed downstream of
286 C12ORF57 and the overexpression of CAMK4 is sufficient to overcome the loss of C12ORF57
287 and rescue the AMPA amplitude phenotype.

288 **Discussion**

289 Our *Grcc10* knockout mice model similar brain phenotypes (seizures, shortened corpus
290 callosum) to those observed in human Temtamy syndrome, caused by mutations in the closely

291 related and poorly characterized human ortholog, *C12ORF57*. Due to the lack of recognized
292 protein motifs or domains in C12ORF57, our *Grcc10* knockout mice provide a novel window to
293 elucidate the precise molecular function of these genes.

294 We showed that loss of *Grcc10* increased AMPA GluA2 in response to chemical stimulus. We
295 also showed that loss of *Grcc10* decreased known excitatory synaptic regulators CREB, Arc and
296 Fos, and that at baseline *Grcc10 -/-* neurons express greater levels of AMPA and have increased
297 mEPSCs. This suggests that C12ORF57 is capable both of regulating the baseline excitatory
298 potential of neurons as well as the neurons dynamic response to overexcitation, suggesting it acts
299 as a neuronal excitatory "rheostat" whose loss leads to an unexpected and dramatic increase in
300 AMPA current and signaling. While the full mechanism and scope of this rheostat function will
301 require further study to elucidate, we believe CAMK4, the binding partner we discovered
302 provides plausible mechanistic insight.

303 The fine tuning of AMPA current would require a protein regulator, which is itself tightly and
304 dynamically regulated. The activation of CAMK4 is a transient and tightly regulated event
305 requiring both Ca^{2+}/calmodulin binding and phosphorylation of the kinase at residue Thr200 by
306 an upstream CaMK kinase (CaMKK) which traffics it into the nucleus (31). Expression of either
307 dominant negative or constitutively active forms of CAMK4, is able to scale up or down
308 excitatory synaptic strength, respectively, and disrupts the cell's ability to dynamically respond
309 to stimuli (31,35,36). As expected, a disruption in CAMK4 activity led to a destabilization of
310 neuronal homeostasis in our *in vitro* murine hippocampal excitatory neuronal model. Loss of
311 *Grcc10* increased AMPA mEPSCs and GluA2 expression and the inability to downregulate
312 excitatory GluA2 in response to chemical stimulus, as observed with CAMK4 dominant negative
313 mutations. Further, similar to the overexpression of the dominant negative version of CAMK4,

314 we observed a decrease in the ratio of nuclear pCAMK4/CAMK4 in our mouse model. Our *in*
315 *vitro* data also supports this observation with the loss of C12ORF57 decreasing downstream
316 CAMK4 signaling through pCREB and ARC. CREB acts upstream of the immediate-early gene
317 *ARC* which is responsible for downscaling excitatory synapses in response to neuronal excitation
318 (26–28). CREB and ARC signaling has been shown to increase endocytosis of surface GluA2
319 expression in response to increased calcium flux from neuronal excitation (9,20). Prior published
320 evidence showed that ARC is involved in synaptic scaling by interacting with endophilin to
321 enhance endocytosis of AMPA receptors, which is crucial for neuronal excitatory/inhibitory
322 homeostasis (20–25). CAMK4 is known to regulate the activity of CREB by phosphorylating its
323 Ser133 residue (37–39). Because sequence analysis of human and murine CAMK4 shows
324 identical calmodulin and autoinhibitory domains, as well as 98.3% amino acid identity between
325 these orthologs, it is likely that our biochemical findings in mice would generalize to humans.

326 Previous studies showed that the autoinhibitory domain of CAMK4 stably associates with protein
327 serine/threonine phosphatases 1 and 2A (PP1; PP2A) to negatively regulate its kinase
328 activity(31,40). These interactions modulate CAMK4's role in homeostatic excitatory synaptic
329 scaling, a mechanism by which neurons adapt their synaptic strength through upregulation or
330 downregulation of surface expression of AMPA receptors (22,35,40). We noted that C12ORF57
331 binds CAMK4 and the presence of the autoinhibitory phosphatase binding domain was important
332 in maintaining this interaction. Further, we also found that C12ORF57 antagonized the PP1CA-
333 mediated decrease in CAMK4 activity *in vitro*. These results give a further plausible mechanism
334 by which C12ORF57 could regulate excitatory synaptic strength through modulation of CAMK4
335 activity by slowing its dephosphorylation.

336 Based on our observations, we propose a model where C12ORF57 protects CAMK4 from
337 dephosphorylation and bolsters its homeostatic role in reining in excitatory synaptic up-scaling in
338 excitatory neurons (**Figure 6**). In this model, the loss of C12ORF57 leads to a decrease in the
339 proportion of active, phosphorylated, CAMK4, reducing negative feedback of excitatory synaptic
340 scaling and increased AMPA expression at synapses. We suggest that these events lead to higher
341 baseline neuronal excitability and increased seizures seen in both TS patients and our murine
342 knockout model. Because sequence analysis of human and murine CAMK4 shows identical
343 calmodulin and autoinhibitory domains, as well as 98.3% amino acid identity between these
344 orthologs, it is likely that our biochemical findings in mice would generalize to humans. It should
345 be noted that this is not the first time CAMK4 activity is implicated in epilepsy in humans;
346 disruptions involving a regulatory miRNA and CAMK4 point mutations have been reported in
347 certain cases (41–43).
348 An important question to address in our model is why previous CAMK4 knockout mice did not
349 present with a similar seizure phenotype (44). It is possible that loss of C12ORF57 in excitatory
350 neurons and a subsequent decrease in the pCAMK4/CAMK4 ratio creates a functional CAMK4
351 knockdown and that cells do not tolerate knockdown as well as a knockout or complete loss of
352 CAMK4 function. Previous work has shown that CAMK4 is sensitive to changes in both
353 subcellular localization as well as relative levels in relation to other CaM kinases which bolsters
354 this hypothesis(37,45,46). In neuronal subsets such as excitatory neurons which have *high* levels
355 of endogenous CAMK4, the levels of other CaMKs such as CAMKI are the principle regulators
356 of neuronal firing, while in neurons with *low* endogenous CAMK4 levels, CAMK4 is the primary
357 regulator of neuronal firing (47). For these reasons we propose the data suggests that it is the

358 relative levels of phosphorylated CAMK4 which cause disruptions in neuronal excitatory
359 homeostasis which are not captured in previous complete knockout experiments.
360 We acknowledge that our model is likely simplified, and that further study is required to elucidate
361 details of how C12ORF57 affects the kinetics, localization, and phosphorylation of various CaM
362 kinases. Also, while we saw no increased NMDA or GABA activity in *Grcc10* KO neurons, we
363 cannot fully determine whether this is due to changes in presynaptic release probability versus
364 purely increased postsynaptic excitation/detection, specifically its effect on AMPA current
365 frequency. Further work is necessary to determine what, if any, effect C12ORF57 has on
366 presynaptic transmission. Additionally, the high perinatal mortality makes it difficult to study
367 certain aspects of the knockout phenotype and limits broader behavioral characterization. The
368 development of a conditional knockout would be helpful to further studying the phenotypic
369 features found in human patients, such as optic coloboma, motor delay, social impairment, and
370 also epilepsy, since complete null mice cannot tolerate EEG placement and monitoring. Another
371 area for future study is that while most mutations currently discovered in human patients involve
372 a loss of function of the start codon, there are several missense, nonsense and splice site mutations
373 reported in compound heterozygotes such as p.L51Q mutations(4,8). Patients with non-initiator
374 methionine mutations have similar phenotypes and severity (epilepsy, agenesis of the corpus
375 callosum and optic coloboma), suggesting that these mutations also result in loss of function of the
376 protein (1,2,4). Further research into specific missense mutations may provide additional insight
377 into key amino acid residues and domains within the C12ORF57 protein.
378
379 In conclusion, we have found that the novel *Grcc10* knockout mouse shares many phenotypic
380 features with Temtamy syndrome patients, making it a suitable model in which to study the

381 function of its human ortholog, *C12ORF57*. We have shown through multiple lines of evidence in
382 murine, human cellular, and *in vitro* models that – a) C12ORF57 binds CAMK4, b) C12ORF57
383 loss decreases CAMK4 phosphorylation and increases mEPSC activity, and c) C12ORF57 loss
384 decreases downstream signaling through the synaptic scaling pathway of CREB, ARC, and GluA2.
385 These findings provide the first evidence for the molecular function of C12ORF57 in neuronal
386 development and homeostasis, as well as a possible explanation for the pathogenesis behind some
387 of the phenotypic features of Temtamy syndrome. Further studies, perhaps using conditional
388 knockout models, are needed to shed further light on additional functions of this protein and tease
389 out its precise role in synaptic homeostasis. Such studies have the potential to give us crucial
390 insight into how C12ORF57 regulates neuronal excitatory synaptic scaling and protects neurons
391 against excessive excitability.

392 **Materials and Methods**

393 **Animal maintenance and generation of G*rcc10* mouse lines**

394 All procedures of animal maintenance and experiments were in accordance with the regulations of
395 and approved by IRB at the University of California San Francisco and in compliance with relevant
396 federal and local laws. All animal breeding and procedures performed in the Richards lab were
397 approved by The University of Queensland Animal Ethics committee and performed in accordance
398 with the Australian Code of Practice for the Care and Use of Animals for Scientific Purposes.
399 Generation of the mouse *Grcc10<tm1.1(KOMP)Vlcg>* line by the Sherr lab was previously
400 described(48,49) .

401 Embryos and postnatal pups were bred from wildtype CD1 time-mated dams at The University of
402 Queensland. The detection of vaginal plug in the following morning after mating was designated

403 as embryonic day zero (E0). Pups are at postnatal day (P0) on day of birth. Tissue collection and
404 fixing was as previously described (9), then post-fixed with 4% paraformaldehyde (ProSciTech)
405 for 2 to 4 days and stored in 1x Dulbecco's phosphate buffered saline (PBS, Lonza) with 0.2%
406 sodium azide (Sigma Aldrich).

407 **Primary Fibroblast Derivation and RT-PCR**

408 Primary fibroblasts were derived from 10mm skin punch biopsies of C12ORF57 patient as
409 previously described by Kisiel et al.(50) All fibroblasts were below passage number 3. RNA was
410 extracted using PureLink RNA mini system (Thermo-fischer 12183018A). cDNA was generated
411 from RNA samples using superscript IV one Step RT-PCR system (ThermoFischer, 12594025).
412 RT PCR was run using the following primers: C12ORF57 F:5'-
413 GGATAACGCCTGCAACGACATG-3' R: 5'-CTTCGTAGGACTTGACCAAGCG-3';
414 GAPDH: F: 5′-GTCTCCTCTGACTTCAACAGCG-3′; R: 5′-
415 ACCACCCTGTTGCTGTAGCCAA-3′

416 **Kainic Acid Treatment**

417 Postnatal day 21 genotyped mice received 20 mg/kg intraperitoneal kainic acid (Sigma-Aldrich
418 K0250) solution dissolved in saline or saline vehicle solution using sterile technique. An observer
419 blinded to mouse genotype recorded time to each Racine stage.

420 **C12ORF57 Antibody generation**

421 C12ORF57 peptide was generated using a full-length cDNA of human C12ORF57 conjugated to
422 N-terminal GST (NCBI9606) produced in BL21(DE3) competent *E.coli.* and purified against a
423 glutathione agarose (GE Lifescience 17075601). Rabbit polyclonal antibody was produced using
424 Thermo Fisher Custom Polyclonal Antibody production.

425 Antibody showed specific bands on western blot at 1:200 dilution in both CMV-C12ORF57-
426 FLAG at expected 17 kD weight and in Grcc10 WT mouse brains and not in Grcc10 KO brains
427 (Supplemental Figure 5).

428 **Cellular Fractionation**

429 Whole mouse brains were Dounce homogenized in fractionation buffer (20 mM HEPES, 10 mM
430 KCL, 2mM MgCL2, 1 mM EDTA, 1 mM EGTA, 1mM DTT) followed by passage through a 27-
431 gauge needle. The nuclear fraction was separated by centrifugation at 720 xg for 5 min.
432 Cytoplasmic fraction was separated at 10 000 xg for 5 min.

433 **Western Blot**

434 Tissue was homogenized with a Dounce homogenizer in RIPA buffer, and lysates were run on a
435 8-20% gradient SDS page. The blots were blocked with Odyssey Li-Cor blocking buffer (Licor).
436 Primary antibodies were followed by an IR fluorescent-conjugated goat anti-mouse and anti-rabbit
437 IgG (1:10 0000, Licor)/ Quantification and IF intensity analysis was done using Odyssey LiCor
438 Image Studio Software v.5.2.5

439 **Antibodies**

440 The following Primary antibodies were used: CAMK4: Invitrogen 8C5B8 (Mouse, MA5-
441 17038,1:1000), pCAMK4 Th200 (Rabbit Invitrogen PA5-37504, 1:1000), pCREB: (Mouse CST
442 87G3 #9197, 1:1000), CREB (Rabbit, CST,48H2, 1:1000), GFP (Chicken, A10626,
443 Invitrogen1:1000), Arc (Proteintech, Rabbit, 16290-1-AP, 1:1000WB), S6 Ribosomal protein,
444 (Rabbit, 5G10, 2217, Cell Signaling Technology) AMPA (6C4, Invitrogen, 32-0300), and CTCF
445 (CST, 28995).

446 The following secondary antibodies were used: IRDye680RD Goat anti-Rabbit IgG (H+L)
447 1:10,000 (Li-cor, 926-68071), IRDye680 Donkey Anti-Chicken (Li-cor, 926-68075), and
448 IRDye800 Goat anti-mouse IgG (Li-Cor, 926-32210).

449 **Co-immunoprecipitation**

450 Mouse brains were homogenized in NP40 lysis buffer (1% NP40, 240 mM NaCl, 5 mM EDTA 50
451 mM Tris ph7.4). 1ug of rabbit anti-C12ORF57 antibody was bound to 2ul of agarose resin and
452 incubated in 1.5ug of total lysate overnight and co-immunoprecipitated using Pierce Co-
453 Immunoprecipitation kit (Thermo Fisher, 26159). Protein was dissociated using low pH Elution
454 buffer (Thermo Fisher, 21104)

455 **Comparative Pull-down experiments**

456 HEK293 cells were co-transfected with C12ORF57-DYKDDDK and CAMK4 constructs in a
457 pCMV backbone. Cells were lysed with 1% NP40 lysis buffer in 1x PBS.

458 1 ug of rabbit Anti-DYKDDDK primary was bound to 20 ul of agarose resin (Pierce, 26159) and
459 incubated in 1.5 ug of total protein overnight. Western blotting was performed as described above
460 and bands were quantified using an Odyssey Licor system as described above.

461 **Hematoxylin and eosin staining**

462 Hematoxylin and eosin (H&E) staining using standard H&E protocols was performed on P0
463 Grcc10 knock-out mouse brains. Dissected brain tissues were sectioned on vibratome (Leica) at
464 50µm thickness in sagittal and coronal orientation.

465 **In situ hybridization**

466 In situ hybridization was performed as described in Moldrich et al, 2010(51). Two sets of Grcc10
467 riboprobes were generated in-house using the primers corresponding to those used in the Allen
468 Mouse Brain Atlas (2015 Allen Institute for Brain Science http://mouse.brain-
469 map.org/experiment/show/386251, Forward primer 1: 5' ACTCAAGCACCGAGTGGC 3',
470 Reverse primer 1: 5' CCTCTGGAACACAAGGGC 3') (Forward primer2: 5'
471 GCTTCCTTTCTGCCTCCTCT 3', Reverse primer 2: 5' CACAGCAGCAGCACACATAC 3').
472 and primers designed with Primer3Plus software. These primers were used to amplify a 459 or 519
473 base pair fragment, respectively, from mouse cortex cDNA. These fragments were purified and
474 cloned into pGEM-T Vector System (Promega). The plasmids were then linearized (NotI or SacII
475 restriction enzyme, New England BioLabs), purified (PCR Clean up Kit, Qiagen), transcribed (Sp6
476 or T7 RNA Polymerase, New England BioLabs) and digoxigenin-labelled (DIG RNA Labelling
477 Mix, Roche) or fluorescein-labelled (Fluorescein RNA Labelling Mix, Roche) to generate the
478 riboprobes.

479 ***In Vitro* CAMK4 assay**

480 CAMK4 kinase activity was measured using ADP Glo System (Promega, V6930). CAMK4,
481 calmodulin, and reaction buffer were supplied by CAMK4 *in vitro* Kinase system (Promega,
482 V2951). C12ORF57-FLAG was transfected into HEK293 cells and purified from whole cell lysate
483 through immunoprecipitation on Anti-DYKDDDK Affinity resin (Genescript, L00432). CAMK4,
484 C12ORF57, and purified recombinant PP1CA (Origene, TA808819) were mixed in equimolar
485 amounts with 25 μM ATP and reaction luminescence was measured on a Tecan Spark for an
486 integration time of 1 sec.

487 ***Primary Hippocampal Neuronal Culture and Transfection***

488 Embryos were removed from pregnant dams at embryonic day 18 (E18). Quick genotyping of the
489 mice was performed by PCR analysis of DNA, extracted from the tail biopsies. Tails were digested
490 in KAPA Express Extract Kit and then template DNA was added to PCR mix containing: 1X
491 KAPA2G Robust HotStart ReadyMix, and *Grcc10* primers (Forward*: 3'-*
492 GCGGACCTCTCTGGGATG Reverse: GCAGCACACATACGAGAACC)
493 After genotyping, hippocampi were dissected in ice-cold Hanks' balanced salt solution (HBSS;
494 Gibco) and were incubated in trypsin/EDTA (Gibco BRL) at 37 °C for 25 min and subsequently
495 transferred to trypsin inhibitor (Worthington) at room temperature for 5 min. After trituration in
496 DMEM/10% FBS solution, cells were counted and plated on poly-L-lysine (Sigma) and Laminin
497 (Gibco) pre-coated cover glass (Harvard Apparatus) at a density of 40.000 cells per 10 mm cloning
498 rings. Cells were maintained in Neurobasal medium (Gibco) containing 1% heat-inactivated FBS,
499 1x B27-supplement (Gibico), 1X Glutamax (Gibco), 15 mM NaCl. Medium was partially
500 exchanged for fresh medium every 7 days. On days 3-5 (days in vitro, DIV), mitotic inhibitor 5-
501 fluoro-2′-deoxyuridine (FUDR, 10 μM) was added to control glial growth.
502 For the transfected experiments, on day 7, *Grcc10+/+* neurons were infected by custom lentiviral
503 particles produced from CW307508 (Origene) with C12ORF57-P2A-GFP under control of a
504 synapsin 2 promoter (Catalog No: CW307508V) at a concentration of 1:100 (0.01) GFP under
505 Syn2 (RC218378LF) or CAMK4-P2A-GFP (Origene Ca MR207505L4V).
506
507 ***In vitro patch clamp recordings***
508
509 Patch clamp measurements were done at DIV 14-17. Before recordings, Neurobasal medium was
510 replaced by HEPES ACSF, containing (in mM): NaCl, 140; KCl, 2.5; HEPES, 10; MgCl2, 2;

511 $CaCl_2$, 2; and dextrose, 10. pH was adjusted to 7.3 with NaOH. mOsm/kg was set to 300. Cultures
512 were visualized under upright microscopy (Olympus, BX51WI) and cells with pyramidal
513 morphology were identified by ×40 water-immersion objective (Olympus) and IR-2000 (DAGE-
514 MTI) camera GFP was identified with 488 nm LED pulse. Whole-cell patch clamp recordings
515 were done from the soma of the pyramidal hippocampal neurons using Axopatch 200B amplifier
516 (Molecular Devices, USA). Cell capacitance and access resistance were monitored throughout the
517 experiments. Signals were acquired with a DigiData-1440A digitizer controlled by pCLAMP-11
518 software (Molecular Devices, USA). Signals were sampled at 10 kHz and low-pass filtered at
519 2 kHz. Borosilicate glass pipettes (4–5 MΩ) were pulled with a horizontal puller (P-1000, Sutter
520 Instrument).
521
522 Miniature excitatory currents (mEPSCs) were isolated from the GABAergic transmission by
523 applying 50 μM $GABA_A$ blocker picrotoxin in ACSF. To capture mEPSCs, voltage-gated Na+
524 channels and NMDA receptor-mediated currents were blocked with 1 μM TTX and 50 μM D-
525 AP5, respectively. Patch pipettes were filled with Cs-based intracellular solution (in mM):
526 CsMeSO3, 135; CsCl, 6; HEPES, 10; phosphocreatine, 10; EGTA, 0.6; Mg-ATP, 3; Na-GTP, 0.5;
527 QX314-Br, 2. pH was set to 7.35 by CsOH and osmolarity to 305 - 310 mOsm/kg. mEPSCs were
528 measured from the holding membrane potential of -70 mV. NMDA receptor-mediated currents
529 were recorded using the same external solution, without magnesium and D-AP5, and with the
530 addition of NBQX to block AMPA currents (10 μM, Tocris). GABA receptor-mediated currents
531 were recorded using external solution without picrotoxin, but with D-AP5, TTX and NBQX. Data
532 analyses were done in Easy Electrophysiology software (Easy Electrophysiology Inc) utilizing a
533 template modeling process for mEPSC detection.

534

535 ***C12ORF57 HEK293 Knockout***

536 sgRNA were generated with the sequence 3'-GATAACGCCTGCAACGACAT-5' and inserted
537 into pCAS_Guide-EF1a-GFP vectors (Origene). HEK293 17T cells were transfected with
538 Lipofectamine 3000 (ThermoFisher, L3000001) and transfection efficiency was determined via
539 immunofluorescence. Lines were picked and maintained with DMEM+10% FBS containing
540 puromycin at 1 ug/ml.

541

542 ***Golgi Cox Staining and dendritic spine density***

543 P18 mouse brains were fixed in formalin and frozen sectioned. Golgi-Cox staining was performed
544 on these neurons utilizing the FD rapid GoligStain Kit (FD Neurotechnologies Inc PK401A).
545 Neurons were chosen at random from slices of mouse cortex and imaged on a Nikon T1 inverted
546 microscope. Dendritic spines were counted and analyzed using ImageJ software plug in Dendritic
547 spine counter.

548 ***Neuronal Surface Staining***

549 Live cultured KO and WT neurons were incubated with a primary antibody directed against the
550 extracellular domain of GluA2. Incubation was conducted at room temperature to slow down
551 endocytosis of the antibody as shown previously (20,35) After incubation with the primary
552 antibody, cultures were washed and fixed for standard immunostaining. GluA2 positive puncta
553 were imaged using confocal microscopy. Their number and fluorescence intensity were quantified
554 over 50 μm of neuronal processes using ImageJ software.

555

556 ***Bicuculline Inhibition***

557 Surface AMPA receptor expression after induction of a chronic increase in postsynaptic activity
558 was assessed by measuring GluR2 surface expression before and after treatment of neurons with
559 bicuculline for 48 hours, as described previously(20,48) .
560
561 ***Statistical analysis***

562 Comparisons between Genotypes:

563 Analysis of Variance (ANOVA): T-test or Mann Whitney Mann Whitney or ANOVA were
564 appropriate was conducted to assess the overall differences between genotypes. When possible, all
565 measurements were done by blinded observers. All T-test were two tailed.

566 Post hoc Analysis: In case of significant differences identified by ANOVA, post hoc tests (Tukey's
567 Honestly Significant Difference test, Sidak's multiple comparison test) were performed to
568 determine specific pairwise differences between groups.

569 Error bars represent ±standard error of the mean (SEM) in all graphs.

570 Statistical software

571 All statistical analyses were performed using Prism version 10.0.0. The significance level (α) was
572 set at 0.05 for statistical tests. Statistical differences are indicated in the figures and tables using
573 the following symbols: $*P \leq 0.05$, $**P \leq 0.01$, $***P \leq 0.001$, $****P < 0.0001$.

574
575 **References**

576 1. Li J, Shivakumar S, Wakahiro M, Mukherjee P, Barkovich AJ, Slavotinek A, et al.
577 Agenesis of the corpus callosum, optic coloboma, intractable seizures, craniofacial and skeletal
578 dysmorphisms: an autosomal recessive disorder similar to Temtamy syndrome. Am J Med Genet
579 A. 2007 Aug 15;143A(16):1900–5.

580 2. Akizu N, Shembesh NM, Ben-Omran T, Bastaki L, Al-Tawari A, Zaki MS, et al. Whole-
581 exome sequencing identifies mutated c12orf57 in recessive corpus callosum hypoplasia. Am J
582 Hum Genet. 2013 Mar 7;92(3):392–400.

583 3. Alrakaf L, Al-Owain MA, Busehail M, Alotaibi MA, Monies D, Aldhalaan HM, et al.
584 Further delineation of Temtamy syndrome of corpus callosum and ocular abnormalities. Am J
585 Med Genet A. 2018 Mar;176(3):715–21.

586 4. Zahrani F, Aldahmesh MA, Alshammari MJ, Al-Hazzaa SAF, Alkuraya FS. Mutations in
587 c12orf57 cause a syndromic form of colobomatous microphthalmia. Am J Hum Genet. 2013 Mar
588 7;92(3):387–91.

589 5. Temtamy SA, Salam MA, Aboul-Ezz EH, Hussein HA, Helmy SA, Shalash BA. New
590 autosomal recessive multiple congenital abnormalities/mental retardation syndrome with
591 craniofacial dysmorphism absent corpus callosum, iris colobomas and connective tissue
592 dysplasia. Clin Dysmorphol. 1996 Jul;5(3):231–40.

593 6. Alfiya F, Jose M, Chandrasekharan SV, Sundaram S, Urulangodi M, Thomas B, et al.
594 C12orf57 pathogenic variants: a unique cause of developmental encephalopathy in a south Indian
595 child. J Genet. 2022;101:30.

596 7. Wang Y, Li M, Luo Y, Zhao X, Liao S, Jiang L, et al. Temtamy syndrome caused by a
597 new C12orf57 variant in a Chinese boy, including pedigree analysis and literature review. Exp
598 Ther Med. 2020 Jan;19(1):327–32.

599 8. Platzer K, Hüning I, Obieglo C, Schwarzmayr T, Gabriel R, Strom TM, et al. Exome
600 sequencing identifies compound heterozygous mutations in C12orf57 in two siblings with severe
601 intellectual disability, hypoplasia of the corpus callosum, chorioretinal coloboma, and intractable
602 seizures. Am J Med Genet A. 2014 Aug;164A(8):1976–80.

603 9. Turrigiano GG. The self-tuning neuron: synaptic scaling of excitatory synapses. Cell.
604 2008 Oct 31;135(3):422–35.

605 10. Franco SJ, Gil-Sanz C, Martinez-Garay I, Espinosa A, Harkins-Perry SR, Ramos C, et al.
606 Fate-restricted neural progenitors in the mammalian cerebral cortex. Science. 2012 Aug
607 10;337(6095):746–9.

608 11. Molyneaux BJ, Arlotta P, Menezes JRL, Macklis JD. Neuronal subtype specification in
609 the cerebral cortex. Nat Rev Neurosci. 2007 Jun;8(6):427–37.

610 12. Bertoglio D, Amhaoul H, Van Eetveldt A, Houbrechts R, Van De Vijver S, Ali I, et al.
611 Kainic Acid-Induced Post-Status Epilepticus Models of Temporal Lobe Epilepsy with Diverging
612 Seizure Phenotype and Neuropathology. Front Neurol. 2017;8:588.

613 13. Tripathi PP, Sgadò P, Scali M, Viaggi C, Casarosa S, Simon HH, et al. Increased
614 susceptibility to kainic acid-induced seizures in Engrailed-2 knockout mice. Neuroscience. 2009
615 Mar 17;159(2):842–9.

616 14. Kokate TG, Cohen AL, Karp E, Rogawski MA. Neuroactive steroids protect against
617 pilocarpine- and kainic acid-induced limbic seizures and status epilepticus in mice.
618 Neuropharmacology. 1996;35(8):1049–56.

619 15. Racine RJ. Modification of seizure activity by electrical stimulation. II. Motor seizure.
620 Electroencephalogr Clin Neurophysiol. 1972 Mar;32(3):281–94.

621 16. Anggono V, Huganir RL. Regulation of AMPA receptor trafficking and synaptic
622 plasticity. Curr Opin Neurobiol. 2012 Jun;22(3):461–9.

623 17. Rogawski MA, Donevan SD. AMPA receptors in epilepsy and as targets for antiepileptic
624 drugs. Adv Neurol. 1999;79:947–63.

625 18. Wenthold RJ, Petralia RS, Blahos J II, Niedzielski AS. Evidence for multiple AMPA
626 receptor complexes in hippocampal CA1/CA2 neurons. J Neurosci Off J Soc Neurosci. 1996
627 Mar 15;16(6):1982–9.

628 19. Schanzenbächer CT, Langer JD, Schuman EM. Time- and polarity-dependent proteomic
629 changes associated with homeostatic scaling at central synapses. eLife. 2018 Feb 15;7:e33322.

630 20. Joseph A, Turrigiano GG. All for One But Not One for All: Excitatory Synaptic Scaling
631 and Intrinsic Excitability Are Coregulated by CaMKIV, Whereas Inhibitory Synaptic Scaling Is
632 Under Independent Control. J Neurosci. 2017 Jul 12;37(28):6778–85.

633 21. Rial Verde EM, Lee-Osbourne J, Worley PF, Malinow R, Cline HT. Increased expression
634 of the immediate-early gene arc/arg3.1 reduces AMPA receptor-mediated synaptic transmission.
635 Neuron. 2006 Nov 9;52(3):461–74.

636 22. Shepherd JD, Rumbaugh G, Wu J, Chowdhury S, Plath N, Kuhl D, et al. Arc/Arg3.1
637 mediates homeostatic synaptic scaling of AMPA receptors. Neuron. 2006 Nov 9;52(3):475–84.

638 23. Kessels HW, Malinow R. Synaptic AMPA receptor plasticity and behavior. Neuron.
639 2009 Feb 12;61(3):340–50.

640 24. Noel J, Ralph GS, Pickard L, Williams J, Molnar E, Uney JB, et al. Surface expression of
641 AMPA receptors in hippocampal neurons is regulated by an NSF-dependent mechanism.
642 Neuron. 1999 Jun;23(2):365–76.

643 25. Shepherd JD, Huganir RL. The cell biology of synaptic plasticity: AMPA receptor
644 trafficking. Annu Rev Cell Dev Biol. 2007;23:613–43.

645 26. Bito H, Deisseroth K, Tsien RW. CREB phosphorylation and dephosphorylation: a
646 Ca(2+)- and stimulus duration-dependent switch for hippocampal gene expression. Cell. 1996
647 Dec 27;87(7):1203–14.

648 27. Soderling TR. The Ca-calmodulin-dependent protein kinase cascade. Trends Biochem
649 Sci. 1999 Jun;24(6):232–6.

650 28. Nonaka M, Kim R, Sharry S, Matsushima A, Takemoto-Kimura S, Bito H. Towards a
651 better understanding of cognitive behaviors regulated by gene expression downstream of
652 activity-dependent transcription factors. Neurobiol Learn Mem. 2014 Nov;115:21–9.

653 29. Bellis AD, Peňalver-Bernabé B, Weiss MS, Yarrington ME, Barbolina MV, Pannier AK,
654 et al. Cellular arrays for large-scale analysis of transcription factor activity. Biotechnol Bioeng.
655 2011 Feb;108(2):395–403.

656 30. Parrish JR, Gulyas KD, Finley RL. Yeast two-hybrid contributions to interactome
657 mapping. Curr Opin Biotechnol. 2006 Aug;17(4):387–93.

658 31. Anderson KA, Noeldner PK, Reece K, Wadzinski BE, Means AR. Regulation and
659 function of the calcium/calmodulin-dependent protein kinase IV/protein serine/threonine
660 phosphatase 2A signaling complex. J Biol Chem. 2004 Jul 23;279(30):31708–16.

661 32. Nakamura Y, Okuno S, Kitani T, Otake K, Sato F, Fujisawa H. Immunohistochemical
662 localization of Ca(2+)/calmodulin-dependent protein kinase kinase beta in the rat central nervous
663 system. Neurosci Res. 2001 Feb;39(2):175–88.

664 33. Tokumitsu H, Brickey DA, Glod J, Hidaka H, Sikela J, Soderling TR. Activation
665 mechanisms for Ca2+/calmodulin-dependent protein kinase IV. Identification of a brain CaM-
666 kinase IV kinase. J Biol Chem. 1994 Nov 18;269(46):28640–7.

667 34. Naz H, Islam A, Ahmad F, Hassan MI. Calcium/calmodulin-dependent protein kinase IV:
668 A multifunctional enzyme and potential therapeutic target. Prog Biophys Mol Biol. 2016
669 May;121(1):54–65.

670 35. Ibata K, Sun Q, Turrigiano GG. Rapid synaptic scaling induced by changes in
671 postsynaptic firing. Neuron. 2008 Mar 27;57(6):819–26.

672 36. Goold CP, Nicoll RA. Single-cell optogenetic excitation drives homeostatic synaptic
673 depression. Neuron. 2010 Nov 4;68(3):512–28.

674 37. Enslen H, Sun P, Brickey D, Soderling SH, Klamo E, Soderling TR. Characterization of
675 Ca2+/calmodulin-dependent protein kinase IV. Role in transcriptional regulation. J Biol Chem.
676 1994 Jun 3;269(22):15520–7.

677 38. Matthews RP, Guthrie CR, Wailes LM, Zhao X, Means AR, McKnight GS.
678 Calcium/calmodulin-dependent protein kinase types II and IV differentially regulate CREB-
679 dependent gene expression. Mol Cell Biol. 1994 Sep;14(9):6107–16.

680 39. Sun P, Enslen H, Myung PS, Maurer RA. Differential activation of CREB by
681 Ca2+/calmodulin-dependent protein kinases type II and type IV involves phosphorylation of a
682 site that negatively regulates activity. Genes Dev. 1994 Nov 1;8(21):2527–39.

683 40. Kasahara J, Fukunaga K, Miyamoto E. Differential effects of a calcineurin inhibitor on
684 glutamate-induced phosphorylation of Ca2+/calmodulin-dependent protein kinases in cultured
685 rat hippocampal neurons. J Biol Chem. 1999 Mar 26;274(13):9061–7.

686 41. Sun J, Cheng W, Liu L, Tao S, Xia Z, Qi L, et al. Identification of serum miRNAs
687 differentially expressed in human epilepsy at seizure onset and post-seizure. Mol Med Rep. 2016
688 Dec;14(6):5318–24.

689 42. Wang Y, Li Z. Association of UGT2B7 and CaMK4 with response of valproic acid in
690 Chinese children with epilepsy. Therapie. 2020;75(3):261–70.

691 43. Zech M, Lam DD, Weber S, Berutti R, Polakova K, Havrankova P, et al. A unique de
692 novo gain-of-function variant in CAMK4 associated with intellectual disability and hyperkinetic
693 movement disorder. Cold Spring Harb Mol Case Stud. 2018 Dec;4(6).

694 44. Takao K, Tanda K, Nakamura K, Kasahara J, Nakao K, Katsuki M, et al. Comprehensive
695 behavioral analysis of calcium/calmodulin-dependent protein kinase IV knockout mice. PloS
696 One. 2010 Mar 1;5(3):e9460.

697 45. Wayman GA, Kaech S, Grant WF, Davare M, Impey S, Tokumitsu H, et al. Regulation
698 of axonal extension and growth cone motility by calmodulin-dependent protein kinase I. J
699 Neurosci Off J Soc Neurosci. 2004 Apr 14;24(15):3786–94.

700 46. Wayman GA, Tokumitsu H, Davare MA, Soderling TR. Analysis of CaM-kinase
701 signaling in cells. Cell Calcium. 2011 Jul;50(1):1–8.

702 47. Cohen SM, Ma H, Kuchibhotla KV, Watson BO, Buzsáki G, Froemke RC, et al.
703 Excitation-Transcription Coupling in Parvalbumin-Positive Interneurons Employs a Novel CaM
704 Kinase-Dependent Pathway Distinct from Excitatory Neurons. Neuron. 2016 Apr 20;90(2):292–
705 307.

706 48. Skarnes WC, Rosen B, West AP, Koutsourakis M, Bushell W, Iyer V, et al. A conditional
707 knockout resource for the genome-wide study of mouse gene function. Nature. 2011 Jun
708 15;474(7351):337–42.

709 49. Okazaki Y, Furuno M, Kasukawa T, Adachi J, Bono H, Kondo S, et al. Analysis of the
710 mouse transcriptome based on functional annotation of 60,770 full-length cDNAs. Nature. 2002
711 Dec 5;420(6915):563–73.

712 50. Böttcher-Haberzeth S, Biedermann T, editors. Skin Tissue Engineering: Methods and
713 Protocols. New York, NY: Humana; 2019. 1 p. (Methods in Molecular Biology).

714 51. Moldrich RX, Gobius I, Pollak T, Zhang J, Ren T, Brown L, et al. Molecular regulation
715 of the developing commissural plate. J Comp Neurol. 2010 Sep 15;518(18):3645–61.

716

717 **Acknowledgments**

718 Thanks to the Linda Richards Lab for their assistance with *in situ* hybrydization lab. Theywere
719 supported by an NHMRC Principal Research Fellowship (GNT1120615).

720 We thank the staff of the University of Queensland Biological Resources (UQBR) animal facility
721 and the QBI Advanced Microscopy and Histology Facilities, for their expertise and assistance in
722 this project.

723 Microscopy support was provided by the Center for Advanced Microscopy and the Nikon Imaging
724 Center at UCSF

725 Suling Wang for providing the illustrations in Figure 6 and Figure 1 Panel 1D.

726 We would like to thank the multiple families and patients who provided samples and participated
727 in our research.

728 **Author Contributions**

729 RJ: drafting/revision of the manuscript for content, Data for found in figures 1-6.

730 MC: drafting/revision of the manuscript for content, data found in figures 2-4 including
731 electrophysiology

732 CM: Contributed data on H&E, immunohistochemistry and in situ hybridizaton.

733 JB: Data on gene expression

734 JL: drafting/revision of the manuscript for content, Data found in supplemental figure 1

735 LR: supervision of laboratory work at University of Queensland, editing manuscript.

736 EU: drafting/revision of the manuscript for content, supervision of laboratory work at UCSF

737 ES: drafting/revision of the manuscript for content, supervision of laboratory work

738 EA and FA: Diagnosed case and established the fibroblast line for human patient

739 **Ethics declarations**

740 Competing interests

741 The authors declare no competing interests.

742

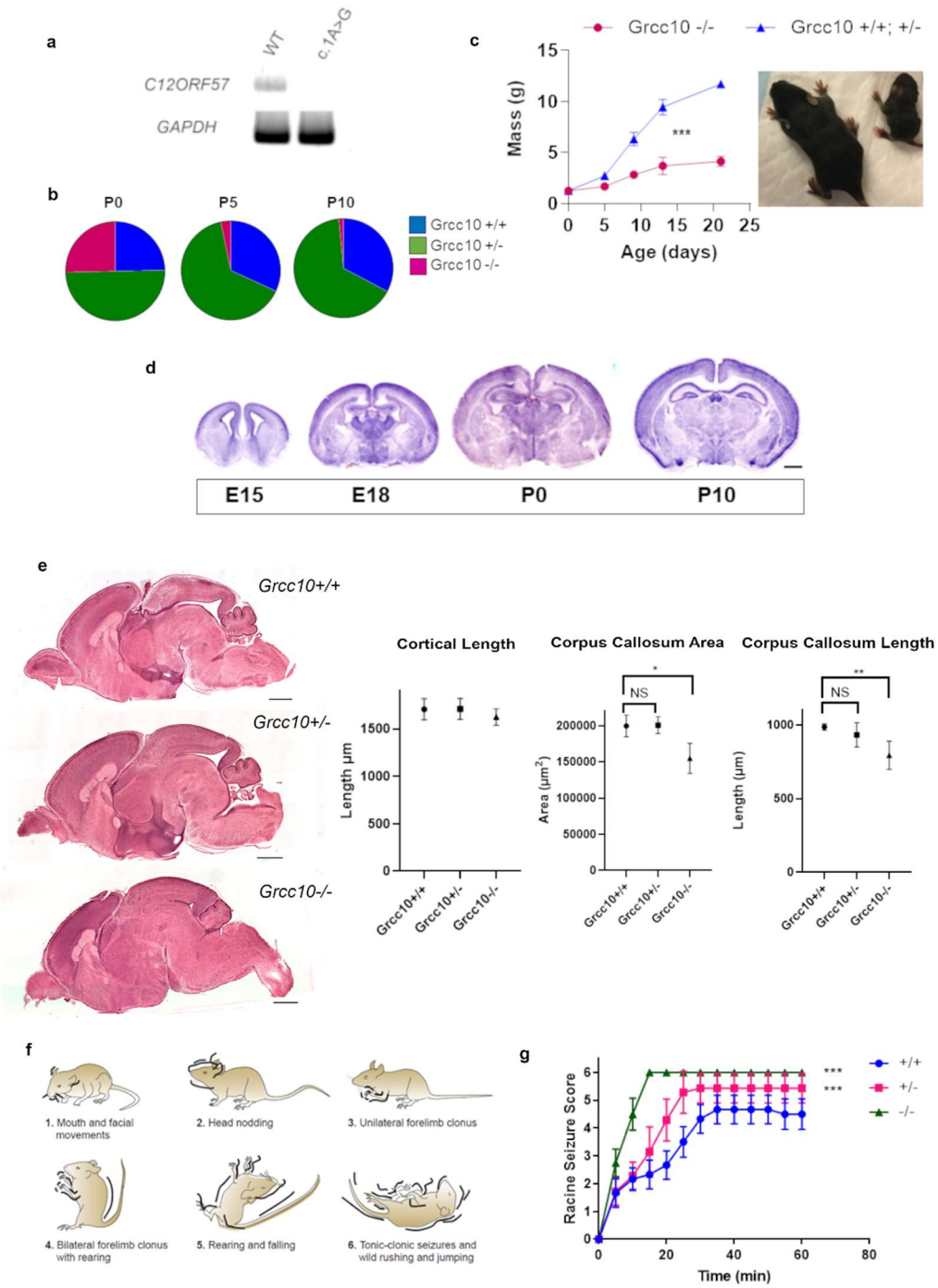

743

744 **Figure 1** *Grcc10-/- Mice Recapitulate the Temtamy Syndrome Phenotype* **a)** RT PCR of
745 C12ORF57 from fibroblasts derived from a human patient with homozygous c.1 A>G mutations
746 in C12ORF57 see loss of transcript when compared to wild type controls. **b)** Ratios of surviving

747 *Grcc10* genotype mice are shown at ages P0, P3, and P21 (N=154, p=0.99, Chi-Square). **c)** Mean
748 body mass (g) are shown for ages P0, P5, P9, P13, and P21 (N=5 for KO mice N=14 for WT and
749 heterozygotes, p>0.0001 ANOVA) **d)** *In situ* hybridization of C12ORF57 shows diffuse
750 widespread expression of *Grcc10/C12ORF57* throughout all brain regions throughout embryonic
751 development. **e)** Representative images of midsagittal slices from *Grcc10+/+, Grcc10+/-* and
752 *Grcc10+/+* mouse brains along with graphs showing mean of cortical length (p=.1127, ANOVA
753 with Tukey post-hoc test), corpus callosum length (p=.017, ANOVA with Tukey post-hoc test)
754 and corpus callosum cross sectional area cross-sectional area (p=.0058, ANOVA with Tukey's
755 post hock). N=6 for KO, N=3 for WT, N=3 for Het.. **f)** Pictographic of Racine stages G) Average
756 Racine stage (x-axis) of mice in time post kainic acid injection (y-axis) for *Grcc10+/+* (blue, N=6),
757 *Grcc10+/-*(pink, N=7) , and *Grcc10-/-*(green, N=4)) (p=.00162, ANOVA with post hoc Tukey).
758 For all Error bars represent SEM. Statistical differences are indicated in the figures using the
759 following symbols $*P \leq .05$, $**P \leq .01$, $***P \leq .001$, $****P < .0001$.

760

761

762

763

764

765

766

767

768

769

770

771

772

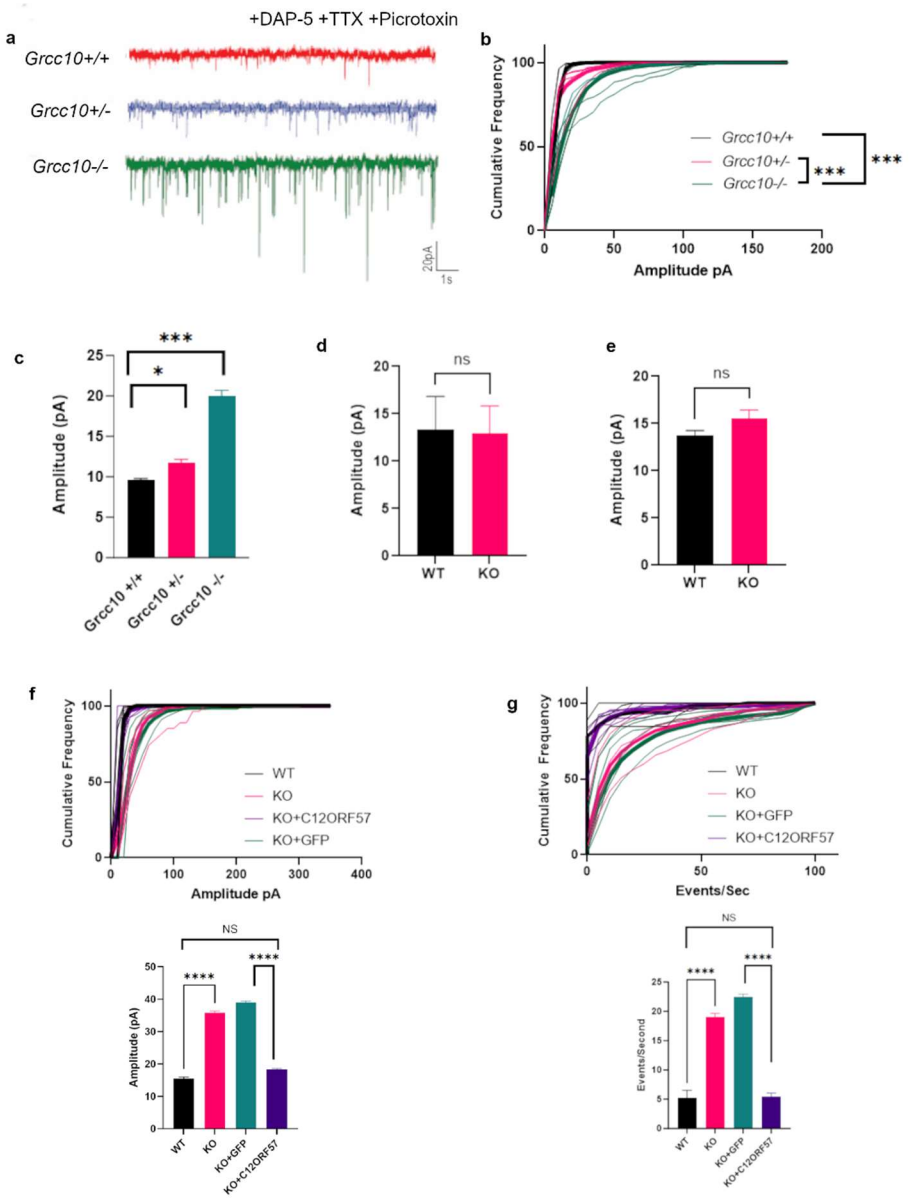

773

774 **Figure 2** *Grcc10 -/- neurons have increased mEPSCs amplitude and frequency* **a)** Representative
775 AMPA mEPSC tracings of *Grcc10* +/+ (WT) neurons (top), *Grcc10* +/- (Het) neurons (middle)
776 and *Grcc10* -/- neurons (bottom). **b)** Graph of cumulative frequency (x-axis) of mEPSC against
777 amplitude in DIV 17 pyramidal neurons. The mean curve of each group is bolded. **c)** Mean AMPA

mEPSC amplitudes (pA) ($p<.0001$, N=5 for each group, ANOVA) **d)** Mean NMDA mEPSC amplitudes (pA). ($p=.20$ N=5 Welch's T-test) Error bars represent SEM. **e**) Mean GABA mEPSC amplitude ($p=.16$, N=5 for each group, Welch's T-test) **f and g)** Upper panels: Cumulative frequency of events plotted against event amplitude (left panel) and the time between events (events/second) (right panel) in DIV17 pyramidal neurons including C12ORF57 transfected rescue (purple) and GFP Control (green). The combined mean of group is represented by corresponding bolded line. Lower panels: Mean amplitude of AMPA mEPSC (left panel) and mean events/second of AMPA mEPSC (right panel). For (**f**) and (**g**), N=5 for each group, ANOVA with Tukey post-hoc test). For all graphs, error bars represent SEMs. Statistical differences are indicated in the figures using the following symbols $*P \leq .05$, $**P \leq .01$, $***P \leq .001$, $****P < .0001$.

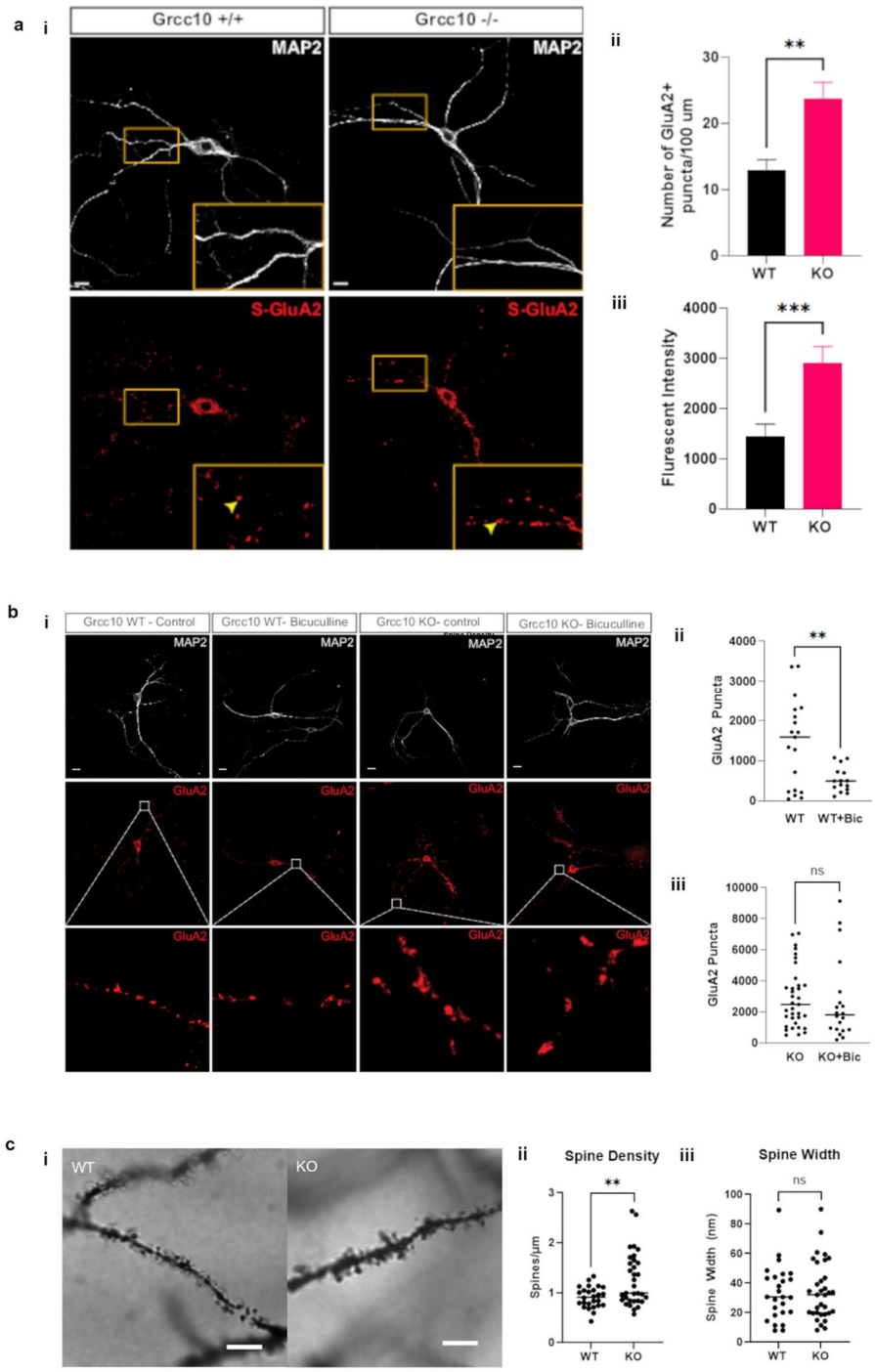

Figure 3 *Loss of Grcc10/C12ORF57 disrupts normal GluA2 expression in primary murine neurons* **a)** (i) Representative images of surface staining of MAP (white, upper panels) and GluA2 (red, lower panels) in *Grcc10* +/+ and *Grcc10-/-* neurons. Insets 2x magnification. Scale bar 20

792 µm. Mean GluA2 fluorescent puncta/100µm (ii) (p=.0024, N=10 both genotypes Welch's T- test),
793 and mean puncta intensity (ii) (p=.0008, N=19 WT, N=35 KO, Welch's T-Test) Error bars
794 represent SEM. **b)** (i) Sample images of DIV 17 hippocampal primary neurons stained for GluA2
795 (red) and MAP2 (white) on both *Grcc10* WT and *Grcc10* KO neurons with and without bicuculline
796 treatment. Scale bar 20 µm. Insets 10x magnification (ii) GluA2 puncta/100 µm on with and
797 without bicuculine, with mean represented as horizontal line (p=.0041, N=19 WT Ctl, N=15
798 WT+bicuculline treated Welch's T-test. Plot of GluA2 puncta/100µm on KO neurons (p=.68,
799 T=.41, df=53, N=20 KO Ctl, N=35 KO+bicuculline treated. Welch's T-Test). Scale bar 20 µm **c)**
800 (i) Representative Golgi-Cox-stained dendrites from *Grcc10* WT and KO cortical neurons (scale
801 bar 5µm). (ii) Plot of spine density (p=.0023, N=33 per group, Welch's T-Test) and (iii) spine
802 width (p=.83, N=33 per group, Welch's T-Test). Mean represented by horizontal line. Statistical
803 differences are indicated in the figures using the following symbols $*P \leq .05$, $**P \leq .01$, $***P \leq$
804 $.001$, $****P < .0001$.

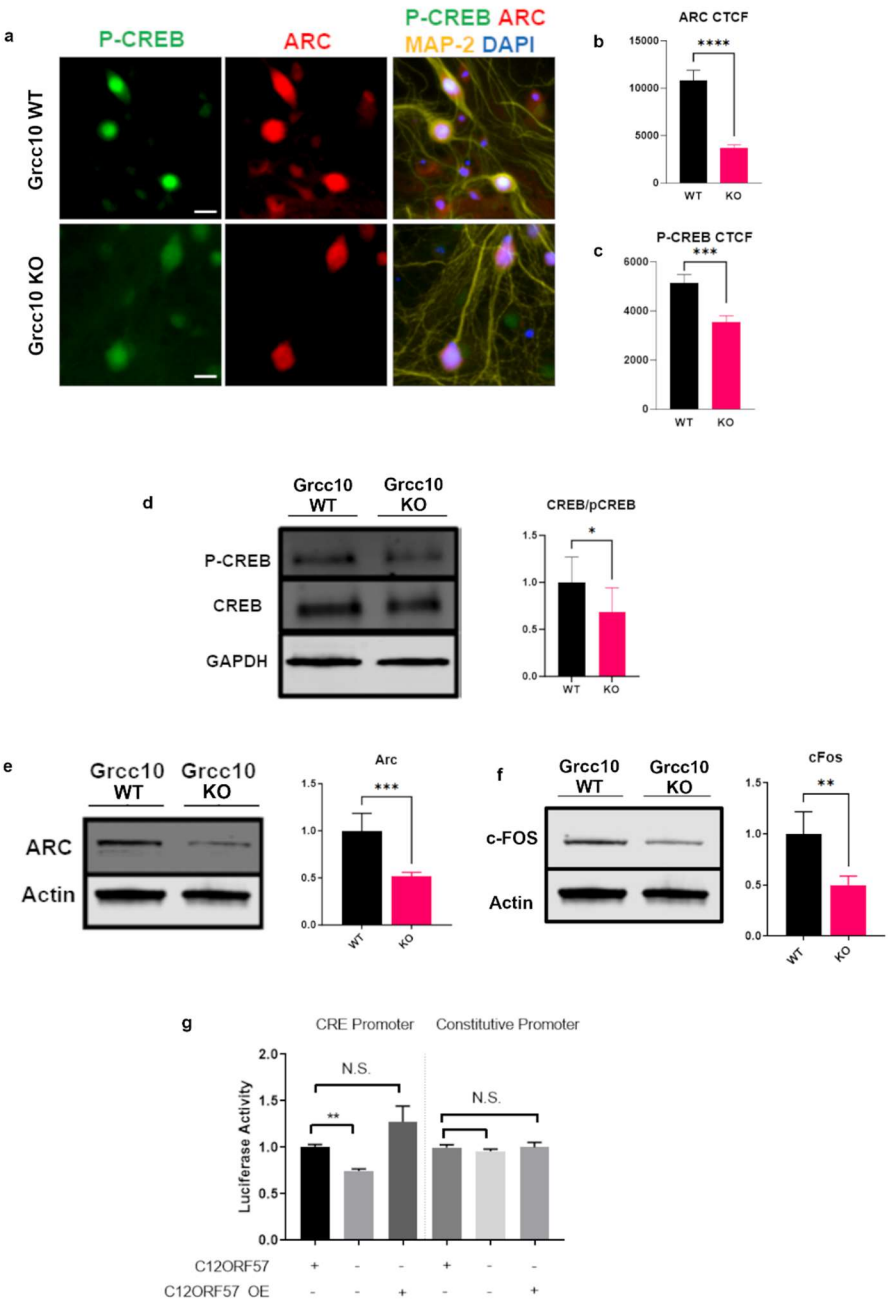

Figure 4 *Loss of C12ORF57 decreases levels of downstream CAMK4 targets* **a)** IHC staining of primary hippocampal neurons from *Grcc10* (upper panels) and *Grcc10* KO (lower panels) mice for phospho-CREB (green, left), ARC (red, center) with overlay of MAP-2 Yellow and DAPI (blue, right) in . Scale bar 5µm **b and c)** Fluorescent quantification of ARC (**b**) (p=.0008, N=20

810 for each genotype, Welch's T-Test) and **p-CREB (c)** (p<.0001, N=24, Welch's T-Test).
811 Normalized means are shown. **d) Left:** Western blot of whole brain lysates of pCREB (top) CREB
812 (middle) and GAPDH controls (bottom). **Right**: Mean ratio of CREB/pCREB fluorescence
813 relative to GAPDH(p=.024, N=10, Welch's T-Test). Normalized to WT Mean. **e) Left:** Western
814 blot of whole brain lysates from *Grcc10* WT and *Grcc10* KO mice with anti-ARC (top) and anti-
815 actin control (bottom) antibodies. Right: Mean ratios of ARC band intensity to actin normalized
816 to mean WT intensity (p=.0036, N=5 for each genotype, Welch's T-Test). **f)** Left: Western blot
817 of whole brain lysates from *Grcc10* KO and WT mice with anti-cFos (top) and anti-actin control
818 (bottom) antibodies. Right: Mean ratio of cFos band intensity to actin normalized to WT mean
819 (p=0.0043, N=5 for each genotype) **g)** Mean relative luminescent signal from Renilla luciferase
820 assay on HEK293 cell lysates normalized to WT control (N=6 for each genotype, Welch's T-
821 Test.). For all graphs, error bars represent SEM. Statistical differences are indicated in the figures
822 using the following symbols $*P \leq .05$, $**P \leq .01$, $***P \leq .001$, $****P < .0001$.

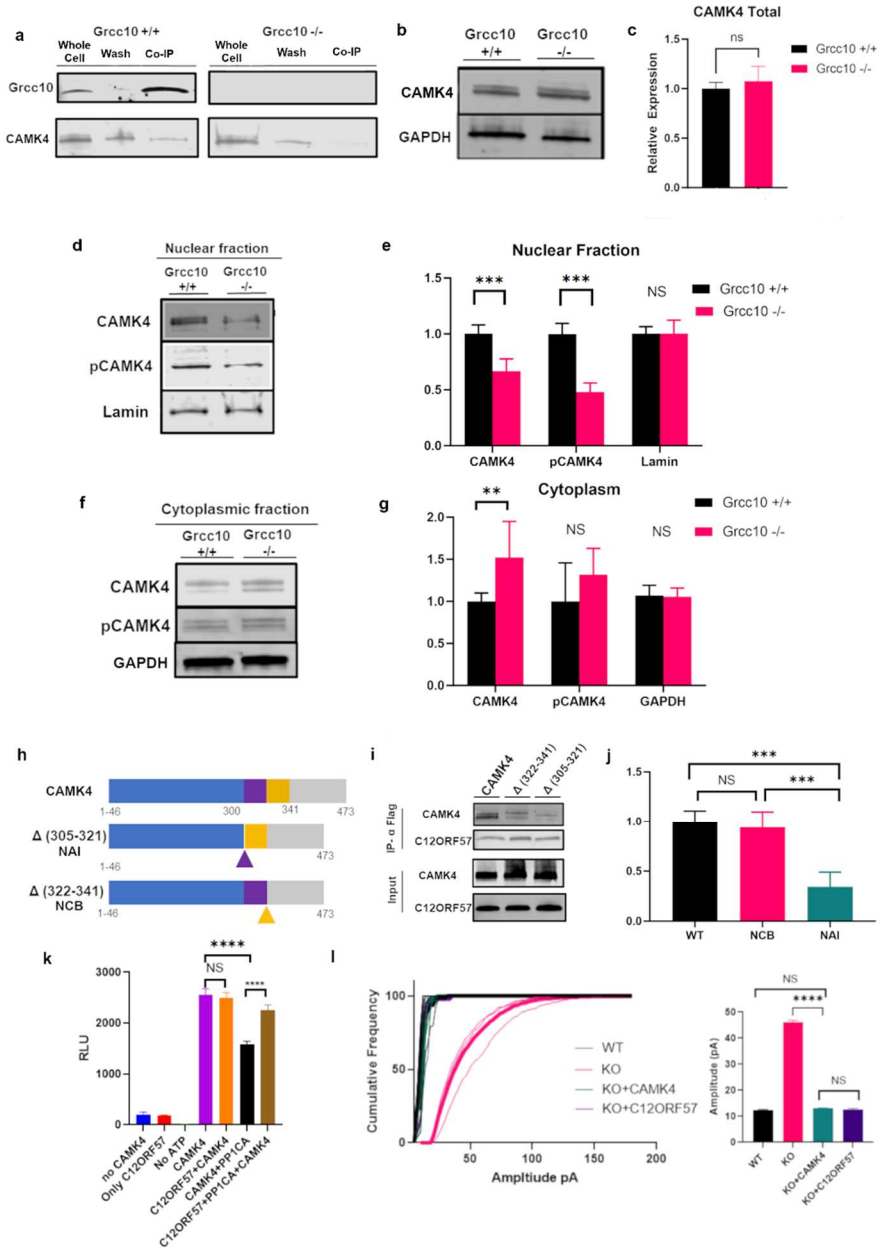

823

824 **Figure 5** *C12ORF57 binds CAMK4 and modulates its phosphorylation and activity* **a)** Western
825 blot showing co-immunoprecipitation of CAMK4 with C12ORF57 from *Grcc10+/+* whole brain
826 lysate (left) with *Grcc10-/-* brain negative control (right) showing no GRCC10 expression or
827 CAMK4 pulldown **b)** Representative CAMK4 and GAPDH western blot bands from brain whole
828 cell lysates of *Grcc10 +/+* and *Grcc10-/-* mice **c)** Mean relative CAMK4 western blot band

intensity normalized to WT (p=.34, N=6 for each genotype Welch's T-Test) Error bars represent SEM. **d)** Representative CAMK4, pCAMK4 and lamin (control) bands on western blot from nuclear fraction of *Grcc10* WT and KO whole brain lysates **e)** Relative CAMK4, pCAMK4and Lamin band intensity normalized to *Grcc10 WT* levels. (p=.001, N=6 for each genotype, 2-way ANOVA with Sidak's multiple comparison test). **f)** Representative CAMK4, pCAMK4 and GAPDH (control) bands on western blot from cytoplasmic fractions of whole brain g) Relative CAMK4 pCAMK4 and Lamin band intensity normalized to *Grcc10* WT levels (p=.016, N=6 for each genotype, 2-way ANOVA, Sidak's multiple comparison test) in KO compared to WT. **h)** Schematic of WT CAMK4 (top) with kinase domain (blue), calmodulin binding domain (purple) and autoinhibitory/regulatory domain (yellow). Construct Δ(322-341) which lacks the autoinhibitory domain (NAI, middle) and construct Δ(305-321) which lacks the calmodulin binding domain (NCB, bottom) **i)** Representative western blot of co-IP of CAMK4 constructs with C12ORF57-FLAG **j**) Relative CAMK4 band intensity between WT, NCB (p=.24, N=8 replicates for each construct, ANOVA) and NAI (p<.0001, N=8 replicates for each construct, ANOVA) CAMK4 constructs.. **k**) Relative luminescence from *in vitro* CAMK4 kinase activity assay for C12ORF57, CAMK4, CAMK4+C12ORF57, CAMK4+PP1CA, CAMK4+PP1CA+C12ORF57, no CAMK4, and no ATP (N=3 per condition, ANOVA). **l**) Left: Graph of cumulative frequency (x-axis) of mEPSC against amplitude (pA) in DIV 17 pyramidal neurons including CAMK4 transfected control (green) KO (pink) WT (black), and C12ORF57 transfected (purple). The mean curve of each group is bolded. Right: Mean amplitude of WT, KO, CAMK4 transfected (KO+CAMK4) and C12OR57 transfected (KO+C12ORF57) (p<.0001, N=6 for each group, ANOVA). For all graphs, error bars represent SEM. Statistical differences are indicated in the figures using the following symbols $*P \leq .05$, $**P \leq .01$, $***P \leq .001$, $****P < .0001$.

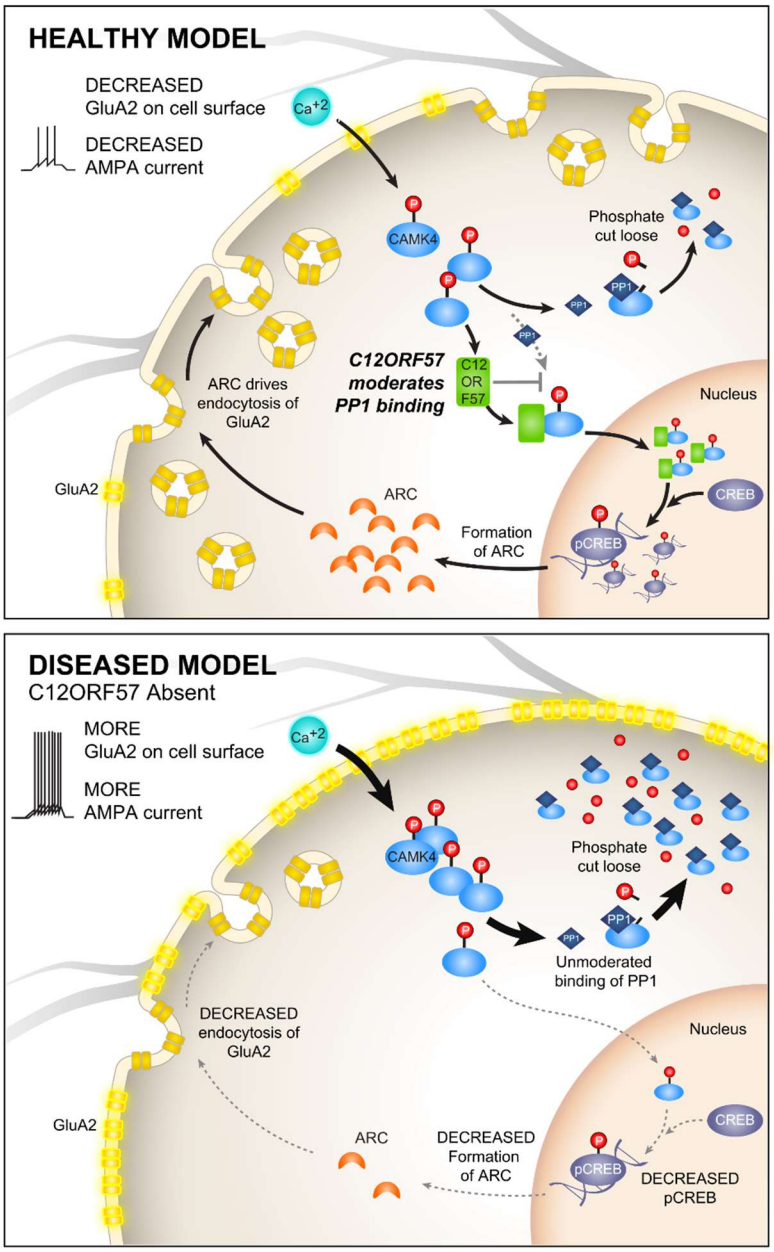

852

853 **Figure 6** *Proposed Model of C12ORF57 Function*

854 Proposed normal function of C12ORF57 (top panel). Under normal conditions C12ORF57 binds
855 CAMK4 and blocks dephosphorylation leading to increased active CAMK4 and activation of ARC
856 and down regulation of AMPA. Loss of C12ORF57 (bottom), where in response to calcium ion
857 influx during depolarization, more CAMK4 is dephosphorylated, and less is able to translocate to

858 the nucleus, decreasing downstream pCREB transcription and ARC transcription resulting in
859 unopposed long-term potentiation, increased GluA2 on cell surface and more AMPA current.